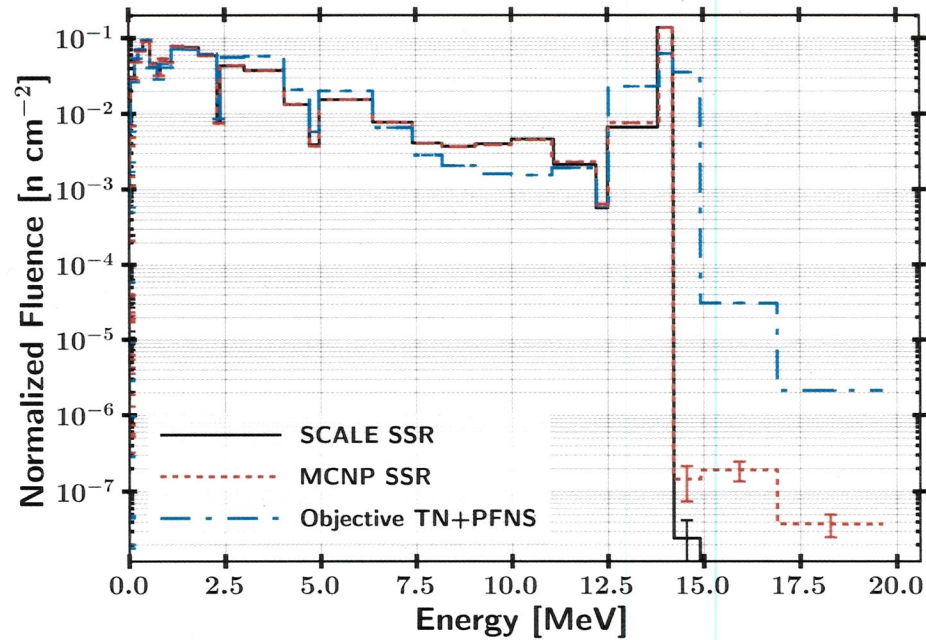


(a) Logarithmic energy scale



(b) Linear energy scale

Figure 34. Neutron fluence for SCALE MAVRIC, MCNP and objective TN+PFNS spectra. Only σ_{stat} is captured for these results.

in the ETA simulations relative
 to the objective spectrum

neutrons; however, this portion of the spectrum only represents 1% of the ETA fluence. The NIF room return and low A spectral shaping components contribute to the majority of this fluence. Additionally, from 7 to 14 MeV there were relatively large differences caused by the method used to generate the TN+PFNS. Godiva, composed of HEU, has very few pathways to populate this region. Inelastic scattering and (n,xn) reactions often completely skip over this portion and there would need to be many elastic scattering events to lower neutron energies to the range from the fusion source. The 14 MeV region disagreement was caused by the lack of attenuation of the source neutrons from weight constraints. Also above 14 MeV, there was a severely depressed neutron flux in ETA. A portion of the disagreement was caused by the mono-energetic source implementation; however, neutrons above 14.03 MeV would also be thermalized through ETA at nearly the same rate.

- define how you use this
 include column
 show difference
 occur + magnitude
- A summary of the fractional fluence of the TN+PFNS and ETA is shown in Table 6. The deviations produced are theoretically discernible within the experimental foil activation portion of the experiment. However, the predictable fission product distribution from each fluence is currently not as precise.

Table 6. 5 energy group fractional fluence for ETA design compared to TN+PFNS

	Fractional Fluence		% diff
Energy Range	ETA Φ	TN+PFNS Φ	
0 - 3 keV	3.24E-04	7.23E-05	
3 keV - 0.11 MeV	4.85E-02	3.80E-02	
0.11 MeV - 6.4 MeV	7.83E-01	8.23E-01	
6.4 MeV - 10 MeV	1.93E-02	1.31E-02	
10 MeV - 19.6 MeV	1.49E-01	1.26E-01	

1.000174 1.0000723

Two statistical tests were conducted for additional confidence in the performance of ETA to spectrally shape the NIF source to the TN+PFNS. The results of the Pearson correlation coefficient and K-S statistic are summarized in Table 7. The in-

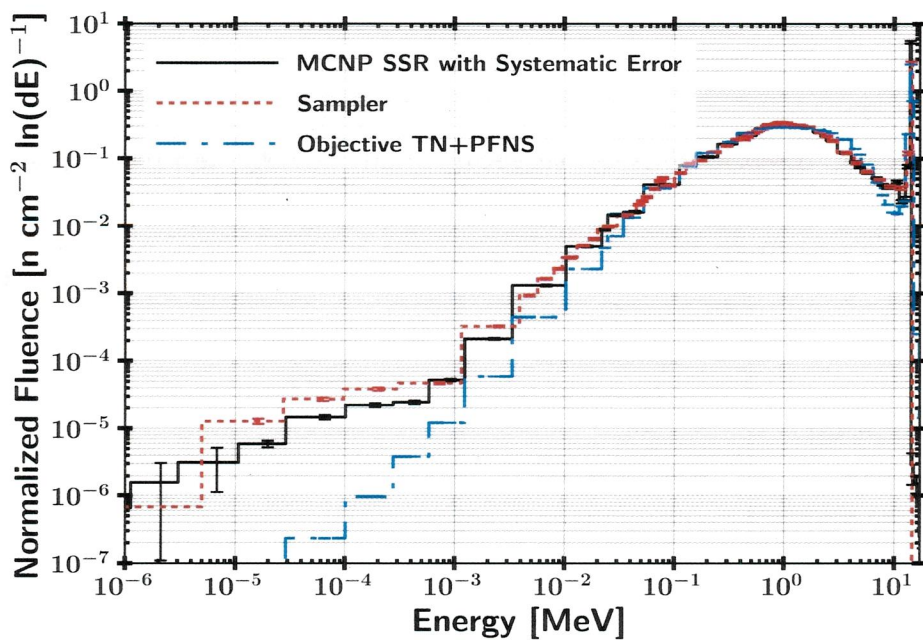
terpretation of the PCC result indicates that no correlation between the data sets was rejected with strong significance, and the K-S statistic indicates the null hypothesis that the samples were drawn from the same distribution could not be rejected.

Describe what this means for the expt and your sims.
Table 7. Statistical test result comparisons between TN+PFNS and ETA performance. The H_0 results indicated that there was a strong correlation between the data sets and the samples were likely drawn from the same distribution. *this belongs in the text not the caption*

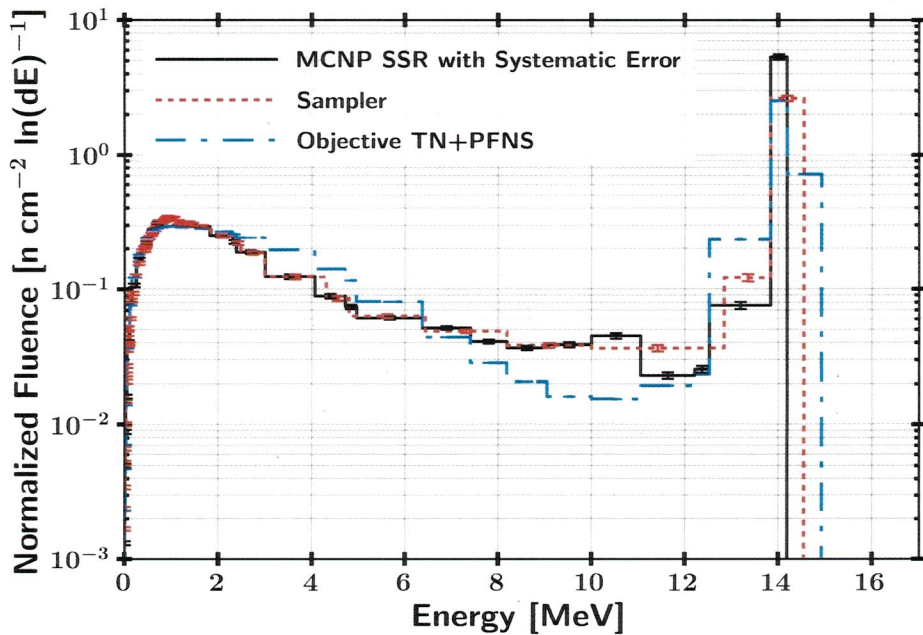
	Pearson Correlation Coefficient (p-value)	K-S Statistic (p-value)	H_0
TN+PFNS versus MCNP SSR	0.90 (p \ll 0.05)	0.11 (p = 0.94)	Pearson - Rejected K-S Failed to Reject
MCNP SSR versus SCALE MAVRIC Mapped SSR	0.9999 (p \ll 0.05)	0.067 (p = 1.0)	Pearson - Rejected K-S - Failed to Reject

???
The nominal value was utilized to determine the similarities between the TN+PFNS and ETA; however, the impact of nuclear data covariance on the neutron transport operated to provide a variability in the expected differential neutron fluence. The neutron flux uncertainty mapped to the 46 group structure DPLUS in comparison with the TN+PFNS is shown in Figure 35. The systematic uncertainty was mapped as described in Section 3.3.5. The fluence is shown per unit lethargy to remove binning artifacts.

The nominal value for each flux bin in Sampler was centered around the unperturbed nuclear data transport as expected because the cross-sections were sampled from a multivariate normal distribution. Additionally, the fluence results highlight the issue of different bin structures and the requirement to estimate the uncertainty for alternative bin structures. The 252 group and continuous energy MCNP results have very similar characteristics; however, the 252 group bin structure is much coarser



(a) Logarithmic energy scale



(b) Linear energy scale

Figure 35. Neutron fluence per unit lethargy scale for Sampler, MCNP and objective TN+PFNS spectra. *in 46 group structure. Include description of error bars in caption*

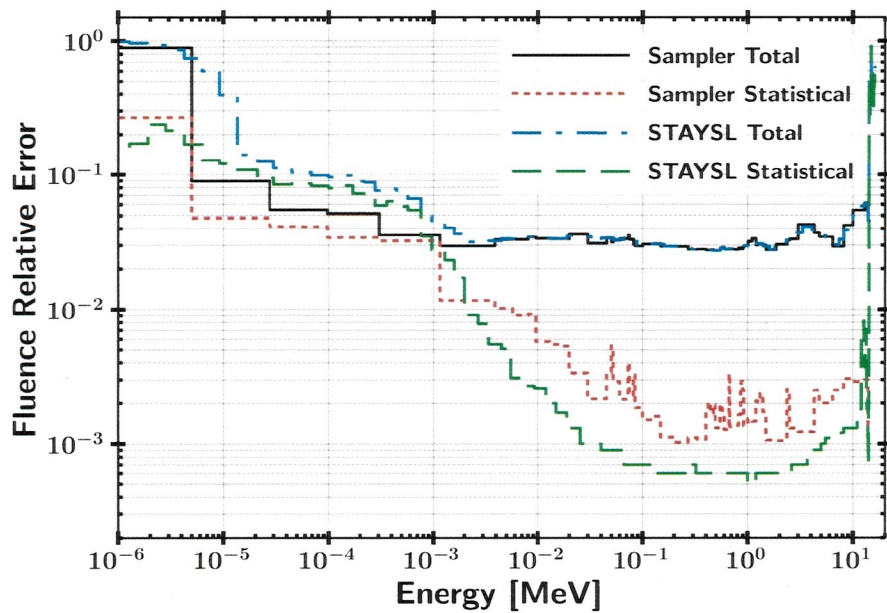
at high energy. The uncertainty results showed approximately 4% uncertainty for a large portion of the spectrum, and rising where σ_{stat} was large. The form of the uncertainty is discussed further in Section 4.1.2. Although the DPLUS library was important for comparing the objective spectrum, the main target group structure was the 129 group STAYSL format.

4.1.2 STAYSL Neutron Fluence with Mapped Systematic Uncertainty

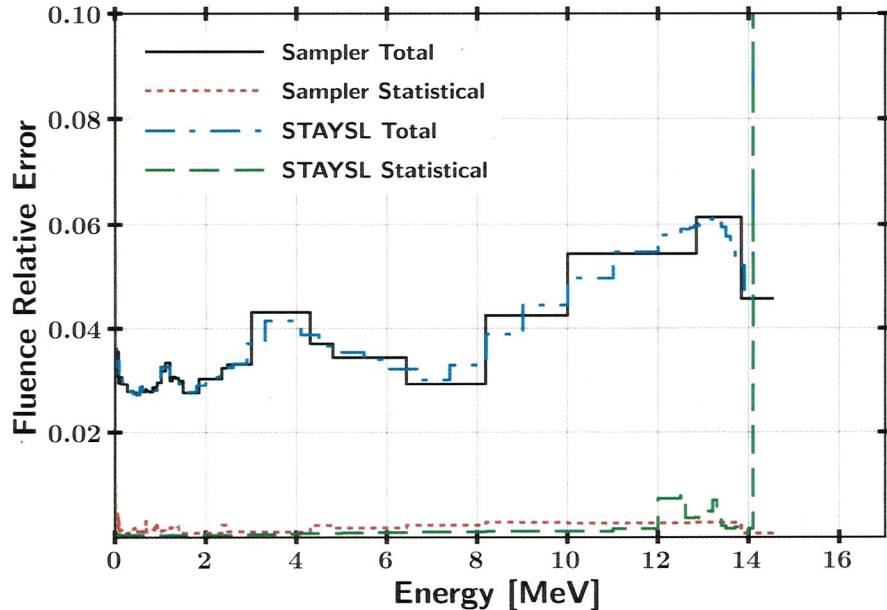
The 129 group STAYSL structure was utilized for the group structure for the neutron flux unfolding. This group structure has fine resolution at high energy which allowed for higher fidelity unfolding of the primarily high energy ETA spectrum. The uncertainty from the Sampler bin structure mapped to the 129 group format is shown in Figure 36.

Present tense

The σ_{sys} was mapped over utilizing the midpoint energy bin linear interpolation. This is a reasonable approximation due to the behavior of the uncertainty as shown in Figure 36. Alternative mappings may have been more appropriate if the uncertainty was not relatively constant. σ_{sys} dominated over σ_{stat} for nearly all of the fluence. At energies close to the source energy of 14 MeV, the total uncertainty was approximately 4-6% which is near the uncertainty of the total scattering cross-section of tungsten and bismuth [at higher energies]. The intermediate energies between 0.01 and 8 MeV comprised a large portion of the neutron fluence and had total uncertainties of approximately 3-4%. Due to multiple pathways to populate the peak of the PFNS, this region of the spectra was impacted less than others. The σ_{stat} and σ_{sys} are nearly the same magnitude at very high energy (> 14 MeV) and low energy (< 1 keV) where the neutron population is reduced. In these regions σ_{stat} is a much more significant contribution to the overall uncertainty, which generally was approximately 10% but approaches 100% at the lowest energy bins.



(a) Logarithmic energy scale



(b) Linear energy scale

Figure 36. Neutron fluence uncertainty from Sampler 252-group structure mapped to the 129 group STAYSL structure. The total uncertainty for Sampler (solid blue) and STAYSL (dash-dot blue) includes σ_{sys} from the nuclear data covariance and σ_{stat} from the Monte Carlo simulation. block

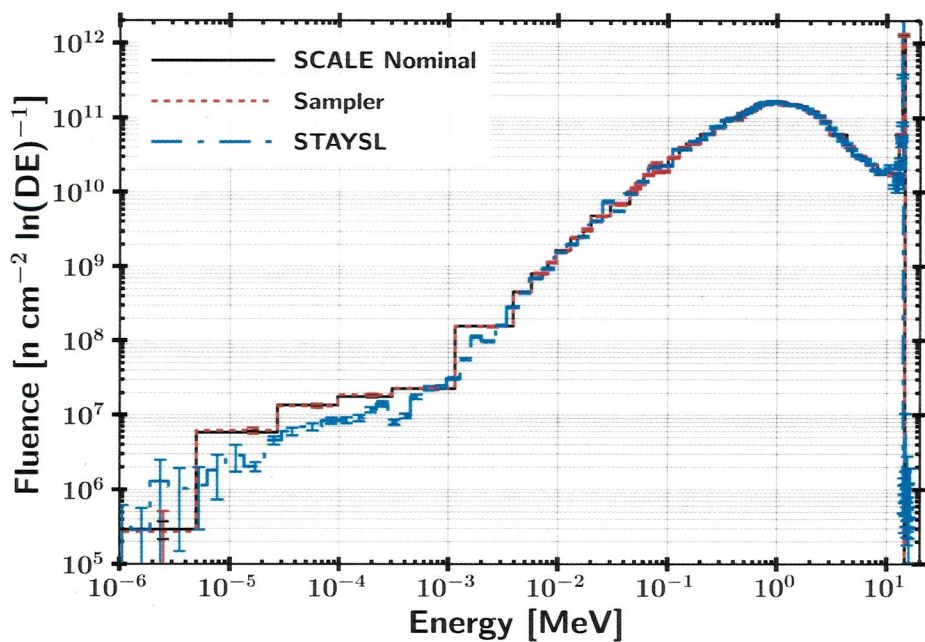
The ETA fluence in the 129-group STAYSL structure with mapped uncertainties is shown in Figure 37 in comparison with the SCALE/Sampler 252-group results from Figure 35. The STAYSL format again matched the characteristics of the 252 group format as seen with the DPLUS format; however, the bin width near the DT fusion source neutrons was smaller resulting in a more defined peak. Up-sampling in this region due to the finer resolution required the assumption that the uncertainty was relatively insensitive to group structure. Additionally, the nominal SCALE 252-group results were compared to the Sampler bootstrapped values, which showed that the mean Sampler value is centered around the nominal unperturbed nuclear data case.

4.1.3 Neutron Flux Timing Profile

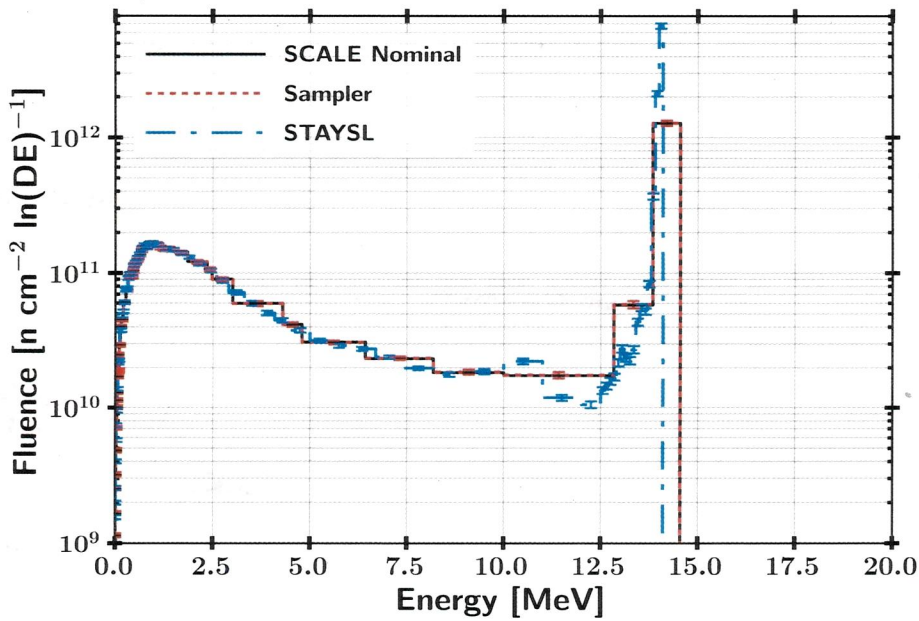
Two major characteristics for a neutron flux environment for use in certification testing are the total fluence of neutrons and the temporal aspect. The incident fluence on the HEU foil was $4.9 \times 10^{11} \text{ n cm}^{-2} \pm 1.4\%$. The time that the neutrons interacted with the volume has implications for applicability of the ETA concept to radiation effects testing. The neutron fluence per unit area from an unshaped point source with a strength of 3.7×10^{15} neutrons at 29 centimeters (distance from source to ETA foils) is $3.5 * 10^{11} \text{ n cm}^{-2}$, so there was an increase in the net neutron population from the spherical divergence. The cumulative fluence on the HEU foil as a function of time is shown in Figure 38.

how was this determined?

The total neutron pulse length in the ETA cavity was approximately 10 shakes or 100 nanoseconds. The uncollided source neutrons arrived at foil in approximately 0.6 shakes, consistent with the time required for a 14.03 MeV neutron to travel from the source to the HEU foil. The source neutrons make up a negligible portion of the total fluence seen by the foils as most are downscattered to nearly produce the objective TN+PFNS. The higher energy neutrons from 2 to 14 MeV took the shortest time



(a) Logarithmic energy scale



(b) Linear energy scale

The
 Figure 37. The 129 group STAYSL fluence compared to Scale 252 group nominal fluence and Sampler values.

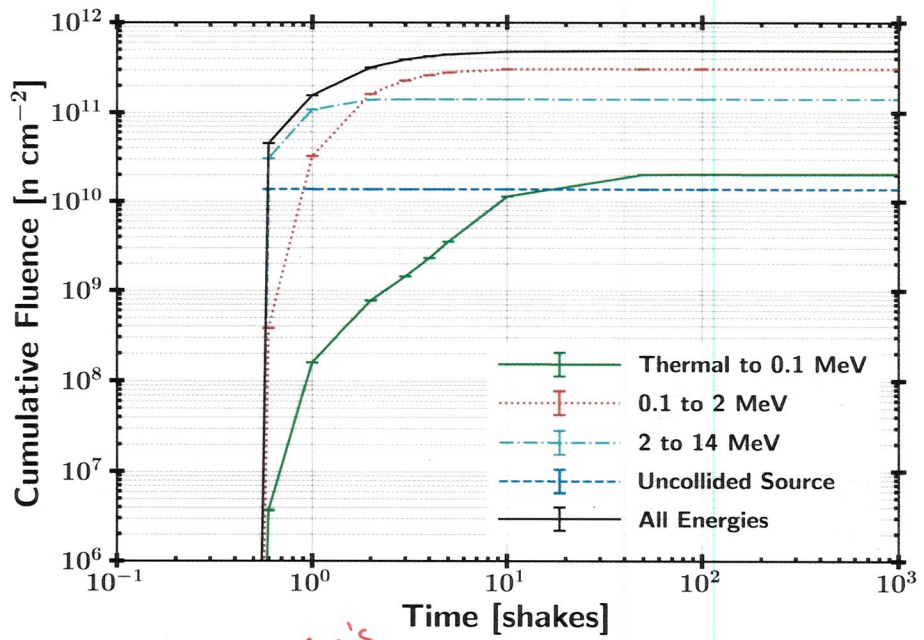


Figure 38. Cumulative fluence on HEU foil as a function of time broken into four broad energy groups.

to arrive at the HEU foil as expected because these neutrons are moving faster and generally experience only a few interactions. The mid-range energy neutrons from 0.1 MeV to 2 MeV encompassed the bulk of the neutron fluence and take a slightly longer time or path to interact with the foils. Finally, the lower energy neutrons below 0.1 MeV take approximately 15 shakes to completely pass through the foils; however, this portion of the spectrum made up a very small percentage of the total fluence. For potential certification testing purposes, a notional electronic component would see the complete fluence in the 100 nanoseconds.

~~4.1.4 Activation Foil Activities~~ *Foil Activation*

The resultant activities ~~Y~~ in the activation foils are presented in Table 8. The individual reactions from Table 1 in Section 3.2.3 ~~were~~ *is* combined with the radioisotope decay constant based on the half-life. The initial activity post-irradiation ~~was~~ *is*

Present tense

compared to the activity at 2 hours, the anticipated time that the foil pack could be removed from the NIF for analysis. The foil activities, on the order of a kilo-Becquerel [kBq] with the exception of the indium foil, are acceptable for gamma-ray spectroscopy using the LLNL facilities. The indium product half-lives are relatively short in comparison to the other isotopes, so a higher activity allows for detection hours later.

Table 8. Activation foil activities predicted with bootstrapped nuclear data covariance uncertainty.

Reaction Product	$\tau_{1/2}$	Initial Activity [kBq]	2-hour Activity [kBq]
⁸⁹ Zr	78.41 hrs	$4.63 \pm 4.7\%$	$4.55 \pm 4.7\%$
⁵⁷ Ni	35.6 hrs	$1.01 \pm 4.8\%$	$0.97 \pm 4.8\%$
⁵⁸ Co	70.86 days	$0.74 \pm 2.5\%$	$0.74 \pm 2.5\%$
¹⁹⁶ Au	6.17 days	$3.78 \pm 4.8\%$	$3.75 \pm 4.8\%$
¹⁹⁸ Au	2.69 days	$2.98 \pm 2.6\%$	$2.92 \pm 2.6\%$
¹¹⁵ In ^{m1}	4.49 hrs	$164 \pm 2.3\%$	$120 \pm 2.3\%$
¹¹⁶ In ^{m1}	54.29 min	$1,094 \pm 3.4\%$	$236 \pm 3.4\%$
²⁴ Na	15 hrs	$13.8 \pm 4.6\%$	$12.6 \pm 4.6\%$
¹⁸⁷ W	24 hrs	$5.79 \pm 4.1\%$	$5.46 \pm 4.1\%$
⁵⁶ Mn	2.58 hrs	$23.5 \pm 20\%$	$13.7 \pm 20\%$

The bootstrapped uncertainty results showed there was a fairly large variance in the foil activities produced. Uncertainty in the radioactive half-life was not propagated as they were comparatively negligible. Most foils result in an uncertainty of a few percent; however, there is high uncertainty (20%) in the ⁵⁵Mn reaction due to relatively large cross-section uncertainty over the activation range compared to other reactions. Additionally, this reaction is impacted by lower energy neutrons where the net transport uncertainty was greater. A histogram of ⁵⁸Ni (n,2n), ²⁷Al (n,a), ¹¹⁵In (n,g), and ⁵⁵Mn (n,g) reactions compiled from the post-processed Sampler results is shown in Figure 39. The remaining histograms deviation from these are minimal; the results indicated a quasi-Normal distribution centered around the

mean value determined from the non-perturbed nuclear data.

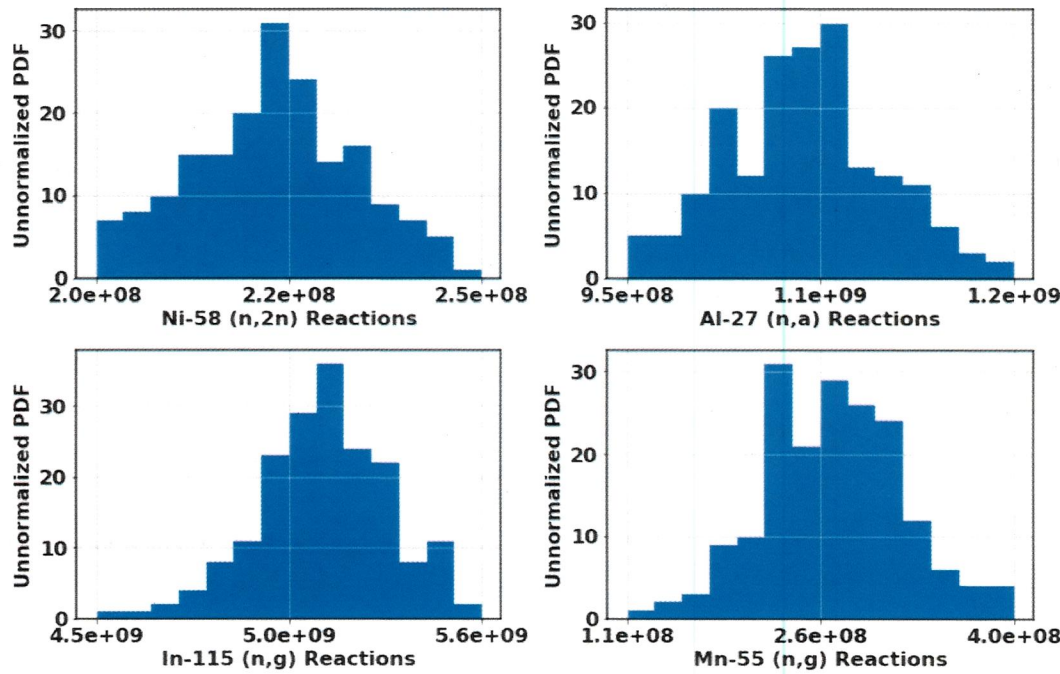


Figure 39. Histograms of several activation foil reactions produced with Sampler results.

The contribution to the total uncertainty from neutron transport, as manifested in the fluence uncertainty, and reaction cross-section uncertainty was determined for the reactions that utilized the IRDFF nuclear data. Reactions that were completed solely in Sampler have this information convolved in the results and are not included in Table 9. The

The uncertainty contributions were largely dominated by the fluence uncertainty as expected since the reactions were chosen for low uncertainty over the activation range. The fluence uncertainty was nearly constant for all high energy threshold reactions covering the TN portion of the spectrum, which was caused by all four reactions having a very similar functional form and energy coverage. In general, non-threshold reactions experienced lower transport uncertainty because the reaction occurs over all energy ranges which reduces volatility in the reaction mechanism.

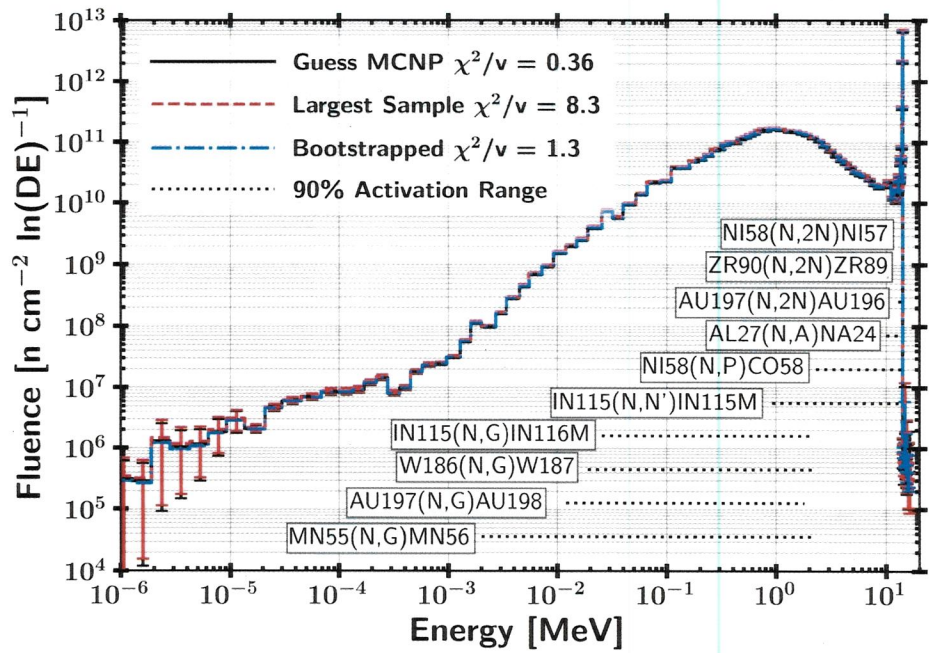
Table 9. Contributions to total uncertainty for activation reactions utilizing IRDFF nuclear data.

Reaction	σ_{total} [%]	Transport σ [%]	Reaction σ [%]
^{90}Zr (n,2n) ^{89}Zr	4.66	4.60	0.78
^{58}Ni (n,2n) ^{57}Ni	4.76	4.57	1.34
^{58}Ni (n,p) ^{58}Co	2.50	2.14	1.29
^{197}Au (n,2n) ^{196}Au	4.84	4.63	1.42
^{115}In (n,n') $^{115}\text{In}^{\text{m}1}$	2.33	1.85	1.42
^{115}In (n,g) $^{116}\text{In}^{\text{m}1}$	3.45	2.59	2.28
^{27}Al (n,a) ^{24}Na	4.62	4.59	0.45

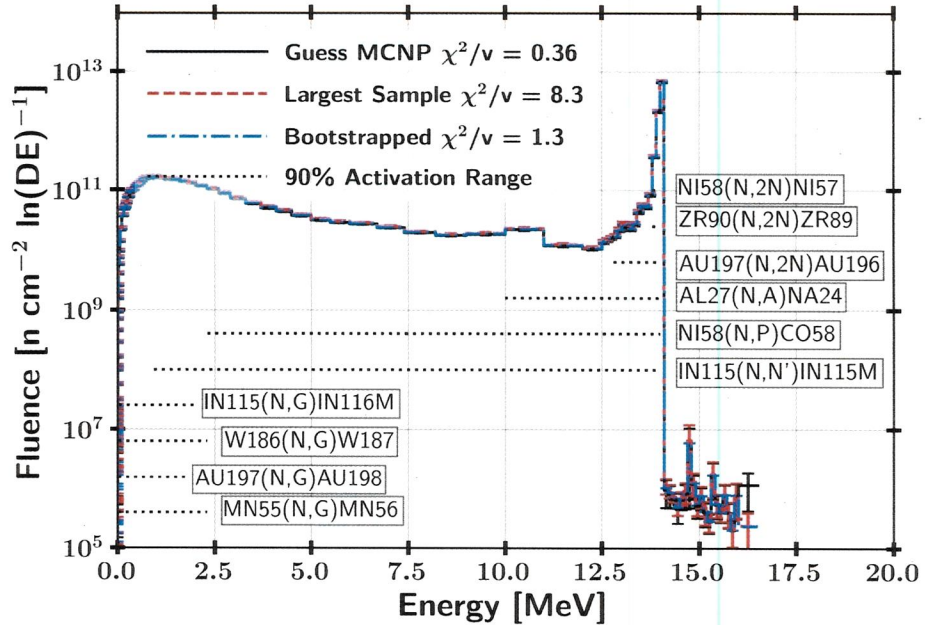
4.2 STAYSL Neutron Flux Unfolding Results

The 129-group STAYSL unfolded spectrum is shown in Figure 40. The results utilized the starting guess MCNP spectrum outlined in Section 4.1.2. The guess spectrum uncertainty provides physics based input to restrict the range of spectrum adjustments performed by STAYSL. STAYSL was executed on all 182 sets of foil activities from Sampler to build ~~up~~ a distribution of possible modeled experimental outcomes. The largest χ^2 trial and bootstrapped neutron fluence from all trials were added to Figure 40 ~~for~~ comparison with the intial guess MCNP spectrum. Additionally, the 5-95% activation ranges for each reaction ~~are~~ ^{ok} shown indicating the region informed in the unfolding procedure by a given reaction.

An important result from the unfolding procedure ~~is~~ defining the region that produced 90% of the activation for each reaction. These regions ~~were~~ ^{are} important for determining the coverage of the activation foil set. Overall, the threshold reactions provided coverage at high energy and ~~were~~ ^{are} mostly saturated by the 14 MeV peak. However, lower energy threshold reactions provided ~~1~~ coverage between approximately 1 and 14 MeV. Finally, the thermal reactions ~~were~~ ^{are} functionally epithermal neutron foils. Although these thermal reactions are not best suited for the epithermal region where the cross-section is low, they proved ~~1~~ beneficial by having a low cross-section at



(a) Logarithmic energy scale



(b) Linear energy scale

Figure 40. STAYSL unfolded spectra per unit lethargy for nominal guess, largest deviation, and bootstrapped values. The 90% activation range represents the saturation region for the foil reactions utilized in the neutron flux unfolding.

high energy where the vast majority of neutrons ^{were} ~~are~~. This low cross-section allowed for higher resolution in unfolding the epithermal portion of the neutron spectrum at the expense of having little coverage at thermal energies.

The χ^2 results indicate that H_0 , that the two sets of data are governed from the expected distribution, could not be rejected for most of the trials with any amount of confidence. The χ^2 was derived from the unfolded activities, not the neutron flux as the flux is not a categorical variable. The p-value reflects the probability of finding a greater χ^2 . The χ^2 for the nominal guess, largest sample, and bootstrapped unfolded activities was 0.36, 8.3, and 1.3 with p-values of 0.96, $\ll 0.05$, and 0.22, respectively. The p-values indicate the probability of achieving a larger χ^2 given the results, so the nominal case was within reasonable expectation while the largest χ^2 value was rejected with strong significance. The bootstrapped activity p-value was closer to the rejection value of 0.05, but the result was large enough to not reject the unfolded activities. It is important to note that the χ^2 values did not include the fluence uncertainty, only the bootstrapped activity uncertainty as outlined in Section 3.4.2. The distribution of χ^2/ν values for the set of trials is shown in Figure 41.

The distribution of χ^2 values peaked around 1; however, a non-negligible portion of the unfolds ^{ing calculations} provided results that rejected H_0 . A few cross-sections may generally increase and others decrease which had a negative impact on the ability to unfold the spectrum. Of the 182 trials, the hypothesis that activities come from the expected distribution was not rejected 81.9% of the time and rejected 18.1% with 95% confidence. ~~✓~~

4.3 Fission Products

The fission product distribution and isotopes ^{were} ~~are~~ the predicted observable quantity reflective of the neutron fluence incident on the HEU sample. First, the fissioning

* This was a simulation w/ known input used to test a procedure that is proposed to be used in the expt. ⁹⁸: there exists a known input spectrum from which all of these results originated. Thus you should be able to quantify the difference btwn the unfolded spectrum & input spectrum. I am missing a plot of STASYL Result compared to TN+RFNS

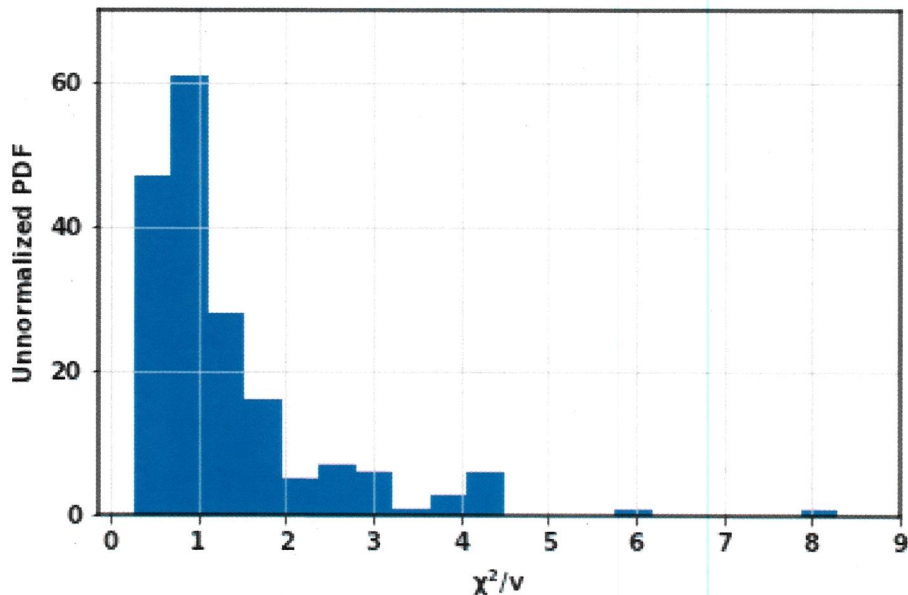


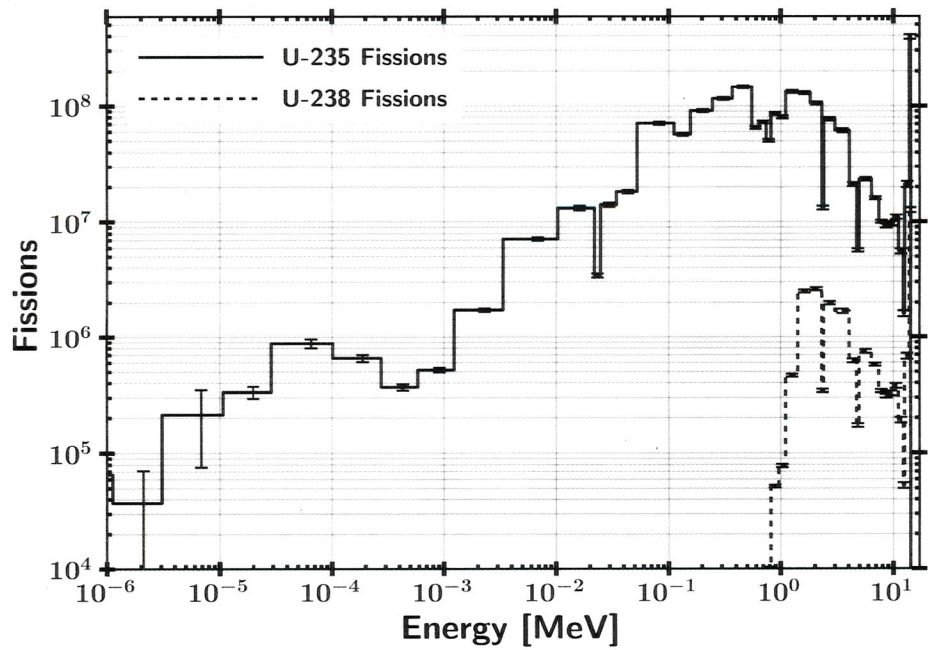
Figure 41. Histogram of STAYSL unfolded ETA spectrum χ^2 for each unfolded trial.

neutron energy spectra are described for ^{235}U and ^{238}U . These spectra are then used with the GEF and Nagy approach⁶ to provided an estimate of the non-volatile gases ? expected to be produced in the HEU.

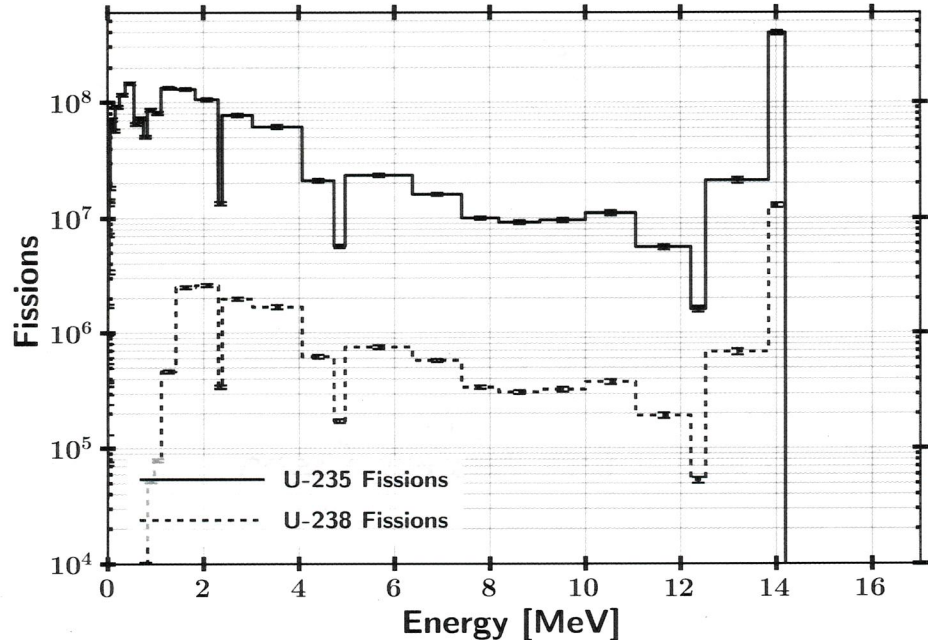
4.3.1 HEU Fission Spectra

The energy dependent neutron fluence convolved with the fission cross-section can be used to determine the fission rate as a function of energy for the various isotopes in the HEU foil. The resultant ETA fissions as a function of energy for ^{235}U and ^{238}U are shown in Figure 42. ETA does not fission

The ^{235}U fissions provide a similar functional form to the ETA sample cavity fluence. However, lower energy fissions comprise a much larger relative contribution to the total fissions, which motivated the necessity for lower statistical uncertainty at lower energies. Still, the majority of the fissions are produced by neutrons above 0.1 MeV in ^{235}U . ^{238}U is a fissionable isotope with a fission threshold at approximately [approximately] The isotope ^{238}U is fissionable with a threshold of ... -



(a) Logarithmic energy scale



(b) Linear energy scale

Figure 42. ETA HEU sample fissions as a function energy.

not sure what is being plotted

*is this # of fission events @ a
given n energy?*

1 MeV and was at a lower number density, so there were significantly less fissions overall. The remaining uranium isotopes were neglected as their contribution was negligible. The spectra here were utilized to provide the compound nucleus energy states for GEF.

4.3.2 GEF

GEF is a useful tool for generating the entire fission product mass chain yields over a large range of fissile and fissionable isotopes. A comparison between the ETA produced fission products and the previously shown ENDF published data is shown in Figure 43. The resultant ETA fission product distribution is on average between the fast and high energy ENDF data. The error associated with the GEF results was large due to the Monte Carlo approach utilized by GEF which included perturbations to the constants utilized in addition to the neutron flux uncertainty.

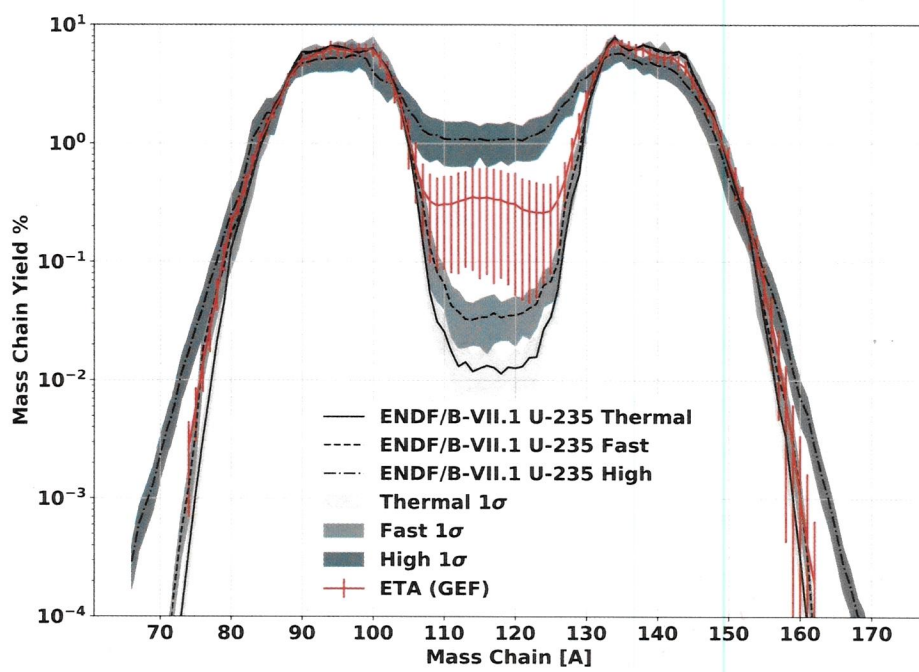


Figure 43. ETA fission product mass chain distribution calculated with GEF in comparison to ENDF values.

The resultant GEF mass chain distribution for ETA and the original objective TN+PFNS are displayed in Figure 44. Overall, there was large agreement in reproducing the fission product distribution expected from the TN+PFNS. The high uncertainty reflects the limited capability to predict mass chain fission products *a priori*.

✓✓✓

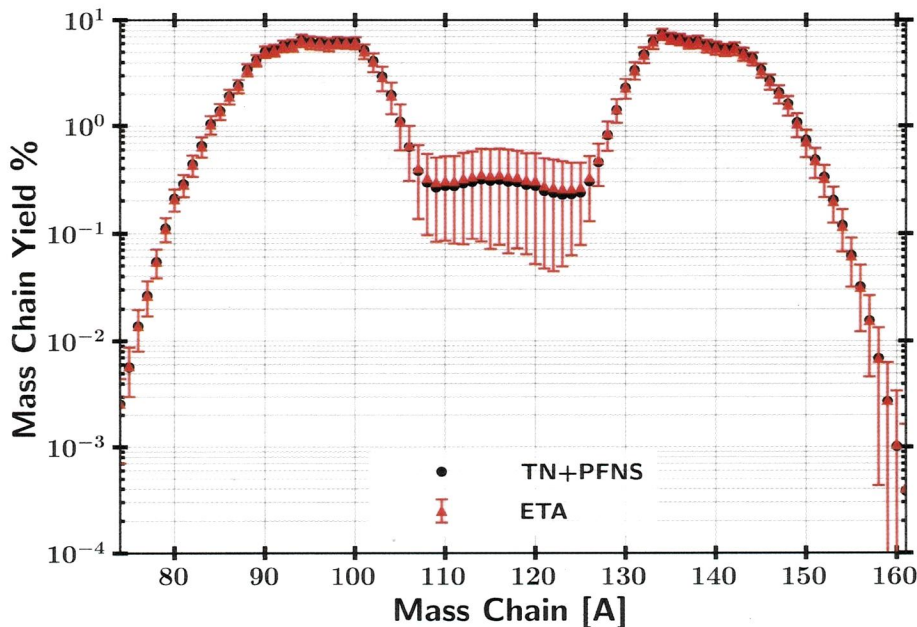


Figure 44. TN+PFNS versus ETA fission product mass chain distributions calculated with GEF values.

The mass chain residual yields comparing ETA to the objective spectrum are shown in Figure 45. There were a few areas of disagreement between the mean value of ETA and the TN+PFNS. The symmetric valley fission products are systematically larger due to the increased high energy flux produced by ETA as highlighted in Table 6. Accordingly, the asymmetric fission products saw an increase. However, neither were substantial compared to the error.

in yield, in error, in ??

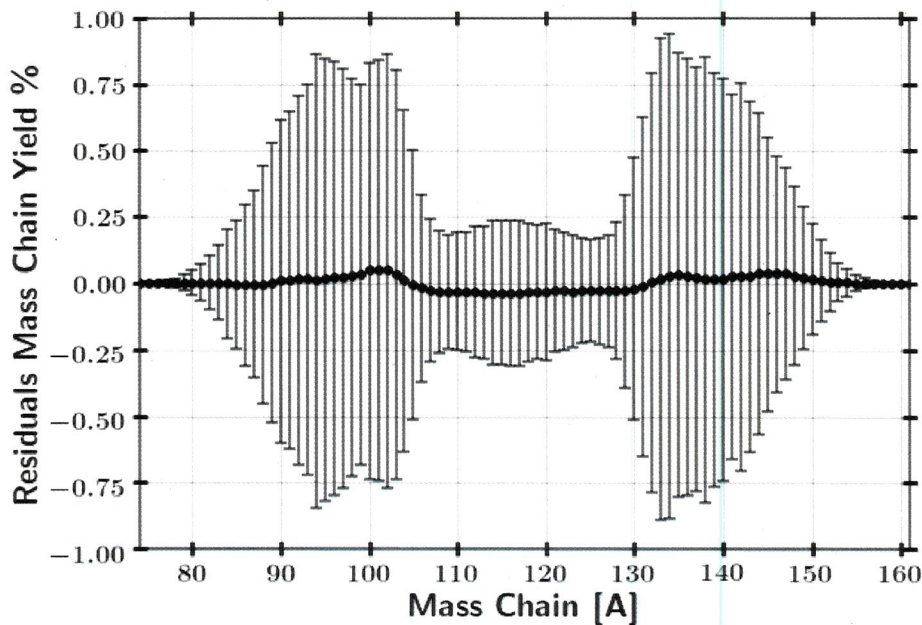


Figure 45. Residual mass chain yields of ETA compared to TN+PFNS from GEF values.

4.3.3 Nagy Fits

The Nagy fit experimental data as a function of incident neutron energy was applied to the ETA fluence. The Nagy fit values represent the cumulative fission product yield for the individual isotope. The resultant fission product yields are compared between ETA and the objective TN+PFNS in Table 10 along with the relative activities compared to ^{95}Zr . ^{95}Zr has a longer half-life and a strong gamma-ray to use as a baseline for comparison to the other fission products.

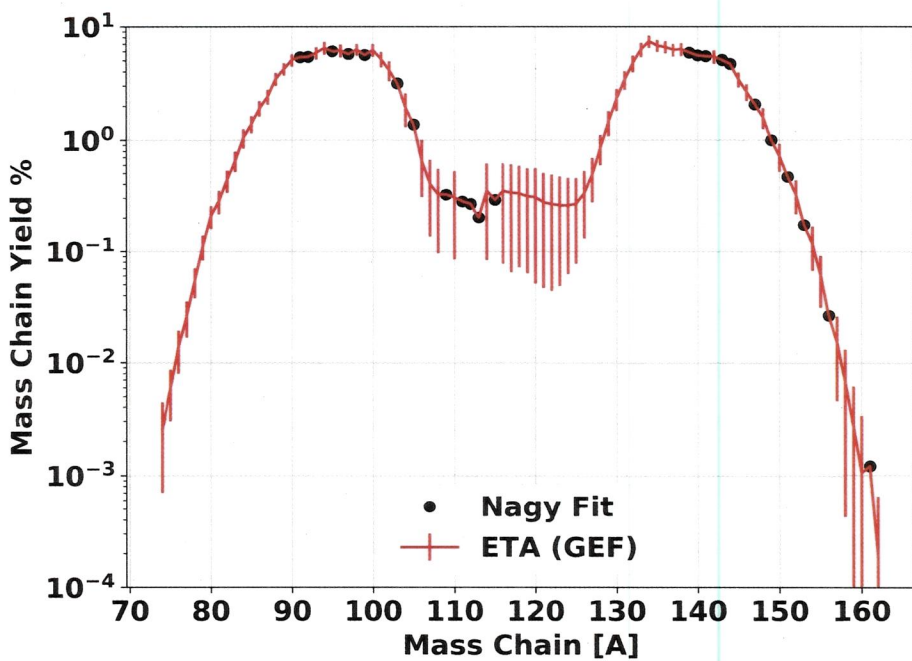
The cumulative fission product yields in Table 10 are often the precursor to the stable state. In the case of additional steps in the decay chain before the stable state, the independent yield of isotopes ~~down the decay chain~~ have negligible yields. Therefore, all of the decay feeding passes through these cumulative fission product isotopes with the exception of ^{132}Te . ^{132}Te is in competition with ^{132}I further in the decay chain. Therefore, the experimental yields, with the exception provided,

Table 10. ETA and TN+PFNS produced Nagy fit cumulative fission product yield from experimental data. The fission product activities were compared to the longer-lived ^{95}Zr

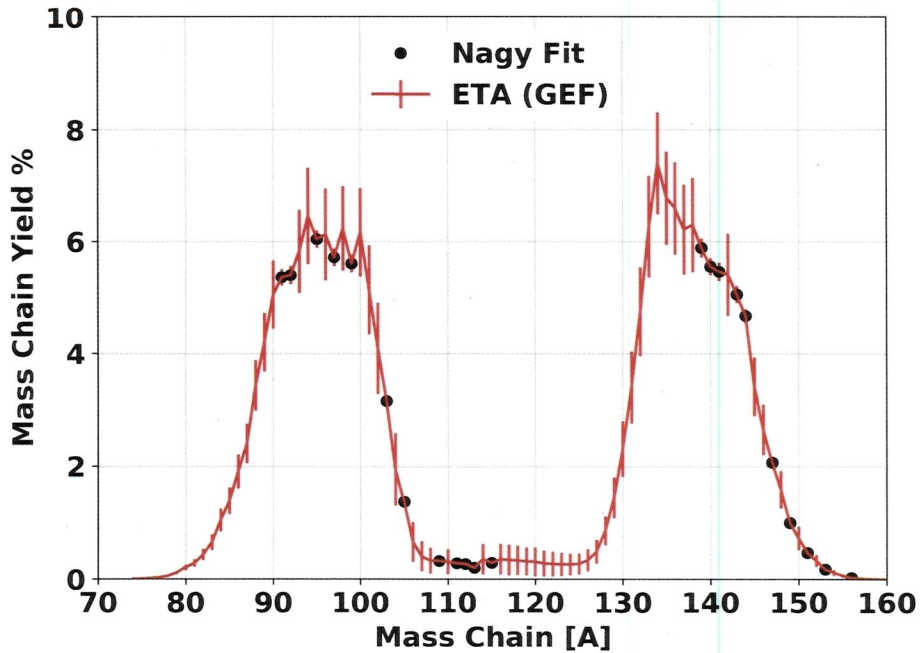
Fission Product	Fission Product Yield [%]		Relative Activity to ^{95}Zr	
	ETA	TN+PFNS	ETA	TN+PFNS
^{91}Sr	5.36 ± 0.15	5.39 ± 0.08	$141 \pm 3.7\%$	$142 \pm 1.7\%$
^{92}Sr	5.40 ± 0.16	5.43 ± 0.10	$517 \pm 3.9\%$	$517 \pm 2.0\%$
^{95}Zr	6.04 ± 0.15	6.07 ± 0.06	$1 \pm 3.6\%$	$1 \pm 1.3\%$
^{97}Zr	5.71 ± 0.16	5.74 ± 0.08	$86.8 \pm 3.7\%$	$86.8 \pm 1.6\%$
^{99}Mo	5.61 ± 0.16	5.63 ± 0.08	$21.6 \pm 3.8\%$	$21.6 \pm 1.7\%$
^{103}Ru	3.15 ± 0.09	3.15 ± 0.05	$0.851 \pm 3.8\%$	$0.847 \pm 1.7\%$
^{105}Ru	1.37 ± 0.05	1.34 ± 0.04	$78.3 \pm 4.6\%$	$76.5 \pm 3.0\%$
^{109}Pd	0.32 ± 0.02	0.29 ± 0.02	$6.00 \pm 6.0\%$	$5.30 \pm 5.3\%$
^{111}Ag	0.28 ± 0.01	0.25 ± 0.01	$0.400 \pm 4.7\%$	$0.351 \pm 3.6\%$
^{112}Pd	0.27 ± 0.01	0.23 ± 0.01	$3.23 \pm 5.3\%$	$2.82 \pm 4.5\%$
^{113}Ag	0.20 ± 0.01	0.18 ± 0.01	$9.54 \pm 6.5\%$	$8.33 \pm 6.0\%$
^{115g}Cd	0.29 ± 0.01	0.25 ± 0.01	$1.38 \pm 5.5\%$	$1.20 \pm 4.8\%$
^{132}Te	4.30 ± 0.12	4.31 ± 0.07	$14.2 \pm 3.8\%$	$142 \pm 1.9\%$
^{140}Ba	5.55 ± 0.15	5.60 ± 0.07	$4.62 \pm 3.7\%$	$4.63 \pm 1.5\%$
^{141}Ce	5.46 ± 0.16	5.49 ± 0.10	$1.78 \pm 3.9\%$	$1.78 \pm 2.0\%$
^{143}Ce	5.06 ± 0.15	5.11 ± 0.08	$39.0 \pm 3.8\%$	$39.2 \pm 1.9\%$
^{144}Ce	4.68 ± 0.13	4.74 ± 0.06	$0.174 \pm 3.7\%$	$0.175 \pm 1.6\%$
^{147}Nd	2.07 ± 0.06	2.08 ± 0.03	$2.00 \pm 3.7\%$	$2.00 \pm 1.7\%$
^{149}Pm	1.00 ± 0.04	1.00 ± 0.03	$4.78 \pm 4.8\%$	$4.79 \pm 3.3\%$
^{151}Pm	0.47 ± 0.02	0.46 ± 0.02	$1,360 \pm 5.0\%$	$1,340 \pm 3.6\%$
^{153}Sm	0.17 ± 0.01	0.17 ± 0.01	$0.950 \pm 6.0\%$	$0.936 \pm 4.7\%$
^{156}Eu	0.027 ± 0.001	0.025 ± 0.001	$0.0187 \pm 5.0\%$	$0.0176 \pm 3.7\%$
^{161}Tb	0.0012 ± 0.0001	0.0010 ± 0.00004	$0.00185 \pm 5.4\%$	$0.00160 \pm 4.2\%$

enable lower uncertainty approximations of the mass chain yields than GEF where experimental data exists. Figure 46 displays the ETA results with Nagy fit data in their given mass chains, which substantially improves the picture of predicting fission product yields. In particular, these isotopes serve as excellent verification data points for the ETA experiment in confirming the ETA fission products.

In a real world scenario, these fallout particles may be collected on the ground



(a) Logarithmic energy scale



(b) Linear energy scale

Figure 46. Experimental predictions of ETA mass chain yields utilizing GEF and Nagy fit data where experimental measurements were taken.

where experimental ~~paper~~ results exist in the literature.

You did not take expt'l measurements.

or air as with the CTBT monitoring. The Department of Defense Fallout Prediction System, DELFIC, can model the fallout distribution on the ground following a nuclear event [97]. A 10 KT fission weapon at ground level was modeled using ^{Weather} data from 16 August 2017 at Wright-Patterson Air Force Base, OH. The ground dispersal in effective fissions per meter square from the 140 mass chain is shown in Figure 47; the 140 mass chain was chosen because the yield does not change drastically with the fissioning system. ETA produces an equivalent number of fissions ^{as} in 0.1 m² of the lowest contour band. As the number of fissions increases, the quality of the sample is more useful. Nevertheless, the modeled ETA performance has promising capabilities to create spectrally accurate fission product debris.

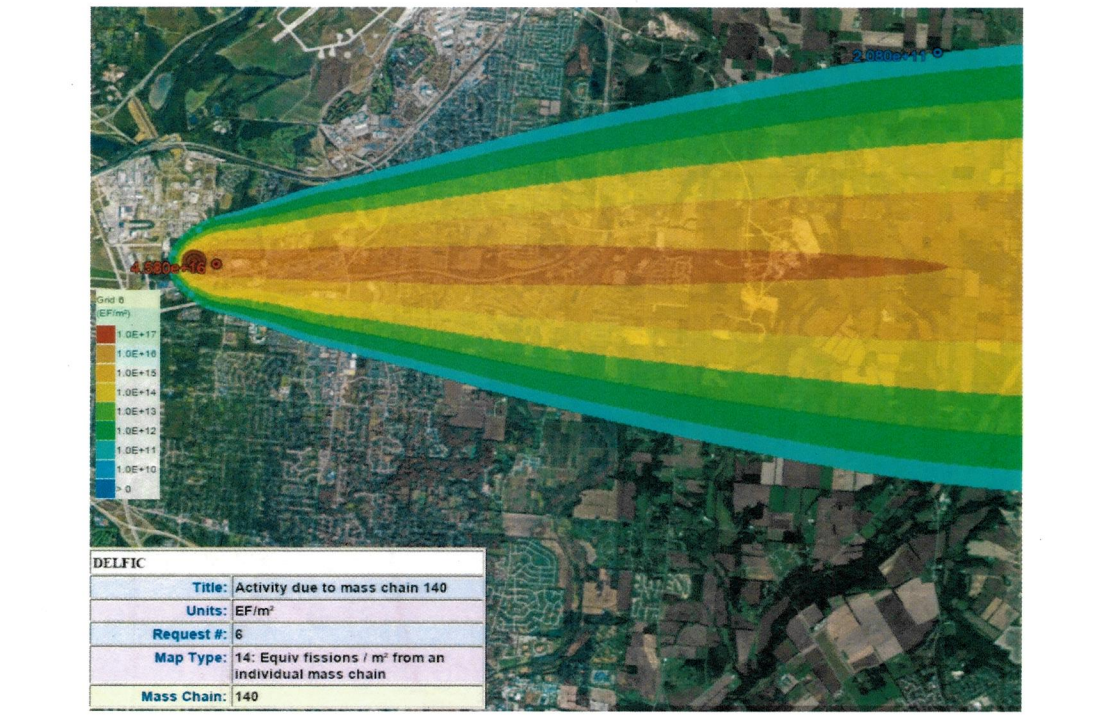


Figure 47. DELFIC calculated fission product equivalent fissions on the ground per unit area from mass chain 140.

5. Conclusions and Recommendations

5.1 Modeled ETA Experiment

ETA can fill the technical nuclear forensics and nuclear weapon certification capability gaps that require an spectrally accurate neutron energy spectrum. The correct fission products associated with the thermonuclear plus prompt fission neutron spectrum (TN+PFNS) will follow directly from the neutron flux which serves as an extremely valuable piece of information for attribution capabilities. Likewise, an accurate energy distribution of neutrons enhances nuclear weapons certification testing credibility. The objective of ~~this~~ ETA research was to determine if the neutron energy distribution in a "typical" boosted nuclear weapon detonation can be produced using spectral modification with an energy tuning assembly (ETA) at the National Ignition Facility (NIF). The goal of ~~this work~~ was determine the expected experimental outcomes of the ETA experiment by incorporating nuclear data covariance analysis. The novel ETA experiment is of high cost, so understanding the full impact of uncertainties, including nuclear data, is important to capture.

The ETA experiment characterization performed in this research indicated a very strong probability of the achieving the surrogate TN+PFNS as designed, but found that the impact of nuclear data uncertainty and covariance on the ETA performance is non-negligible. The neutron transport impact on the fluence uncertainty was assessed with the SCALE Sampler sequence with 182 trials and found to be on the order of a few percent over the broad spectrum; however, the systematic uncertainties increased at lower neutron energies. The statistical testing performed on the ETA produced neutron fluence compared to the TN+PFNS showed large spectral agreement. The Pearson correlation coefficient between the nominal results and TN+PFNS was 0.9 which indicates strong agreement between the spectra. Also, the Kolmogorov-

Smirnov statistic comparing the cumulative distribution functions between the nominal results and TN+PFNS was 0.11 which has a p-value of 0.94 indicating the two samples were drawn from the same distribution with high confidence.

The ETA served as a candidate for neutron induced radiation effects testing for nuclear weapon certification. The fluence of neutrons in the ETA sample cavity was $4.9 \times 10^{11} \text{ n cm}^{-2} \pm 1.4\%$, which is near a useful range for testing ($10^{12} - 10^{14} \text{ n cm}^{-2}$). The neutron pulse length for ETA was approximately 10 shakes which may be useful depending on experimental timing requirements; however, the combination of fluence, spectrum, and timing provides a unique testing capability. However, it is worth noting that the current ETA design was not directly optimized to provide a nuclear weapons effects testing capability, and the TN+PFNS is not representative of the transmission neutron flux through material or atmosphere. Nonetheless, these results provide a step forward in progress towards a short pulse neutron source. *suitable for the nuclear weapon community.*

*is expected to be
was calculated to be
be
tie back
to intro list
of alternate
domestic n°
sources*

The foil reaction uncertainties utilized the International Reactor Dosimetry and Fusion File (IRDFF) v.1.05 nuclear data library and were sampled according to a multivariate normal distribution. The propagated nuclear data uncertainty on the foil activities resulted in uncertainties on the order of a few percent for all but the ^{55}Mn (n,γ) reaction where the nuclear data was not as well characterized and the systematic error was found to be 20%. The foil activities produced in the ETA cavity were found to be sufficient sources for gamma-ray spectroscopy post-shot at the NIF.

Additionally, the activation foil pack designed to unfold the neutron energy spectrum in the ETA experiment was found to have broad neutron energy spectrum coverage and multi-reaction coverage at epithermal energies, typically a trouble area for unfolding. The STAYSL unfolded results on each of the 182 Sampler trials provided an 80+% probability of being able to successfully unfold the neutron spectrum

We should have
a longer talk about
this sometime in the
CCF -

with the foil set and the modeled spectrum based on the χ^2 of each unfolded trial. ✓

In the context of technical nuclear forensics and attribution capabilities, the observable quantity is the fission product distribution created from the neutron flux interaction with the fissile material. ETA's modeled performance produced $2 \times 10^9 \pm 1\%$ fissions which is near the order of those collected in forensics ground samples. Selected fission products were analyzed with the General Description of Fission Observables (GEF) code and experimental data was used to create energy dependent Nagy fits. The fission products produced by ETA have an equivalent cumulative fission product distribution to the defined objective TN+PFNS with current predictive capabilities. Spectrally accurate fission product distributions are extremely important to nuclear forensics and attribution linked to counter-proliferation efforts and attribution techniques for deterrence.] ?? word missing

5.2 Future Work

The NIF experiment to validate the ETA is planned for late 2019. The future work related to the analysis performed here will compare the experimental outcomes to the predicted reactions. The experimental results create a verification of the nuclear data covariance analysis technique utilized. Updates to this analysis will include changes to the fielded configuration of ETA for the experiment. The tools generated for this work will heavily expedite the re-analysis.

Although ETA is a huge step forward for developing synthetic weapon debris, improvements will be made to develop a second generation ETA. A THErmoneuclear and prompt fission Neutron spectrum energy tuning Assembly (ATHENA) will be developed to generate a more representative neutron spectrum. Additionally, facility improvements to the NIF and updated constraints will be incorporated to increase the optimization. The goal of ATHENA is to develop a new ETA design to increase

the ETA efficiency to produce $\sim 10^{12}$ fissions. Attaining a higher number of fissions is extremely important to create better quality samples and achieving better detection of low production fission products.

Finally, the goals have focused on generating a spectrally accurate neutron source and the generation of fission products; however, a real-world scenario deposits as nuclear fallout and includes fractionation based on the physical properties and chemistry of the fission products. A fractionation technique can most readily focus on refractory fission products with low condensation points, as apposed to volatile mass chains as many of these are gases which may be lost in chemical separations. Incorporating the fractionated synthetic fission product debris into a matrix representative to a nuclear forensics collection would be of great benefit to technical nuclear forensics training and exercises.

I have
questions about
the longevity of such
a repository and its
usefulness as a reference for
this doc 5-10 yrs from now.

Appendix A. Reproducibility

All of the underlying documentation presented for this research is available in an online repository at https://github.com/nickquartemont/NIF_ETA. Several Python 2.7 scripts were created to read in data files produced from Sampler as an alternative to the built-in version in SCALE to work more with the data. Much of this work may prove useful to others needing the tools created for this work with some simple modifications. The organization of the repository follows the major efforts taken for the research. A list of tools that will be most beneficial for others is below. The main page includes the thesis, experiment collaboration, documents, briefs, and the models used.

- Sampler Tools

(https://github.com/nickquartemont/NIF_ETA/tree/master/Models/Scale/ScalePy)

Instructions for utilizing the tools to read in and analyze response functions from Sampler are described in readme.txt. This tool can be directly utilized for response functions text files generated by SCALE Sampler. The Sampler files are saved to a pickle file containing the dictionary dataframe of the energy dependent response data.

- STAYSL with Sampler Trials

(https://github.com/nickquartemont/NIF_ETA/tree/master/Models/STAYSL_Unfold/SAMPLER)

This tool utilizes the Sampler dataframe to generate independent trials for STAYSL and build up the distribution of unfolded responses. STAYSL_Analysis.py provides the user interface for the tool.

- Fission Product Estimation with GEF

(https://github.com/nickquartermont/NIF_ETA/tree/master/Models/FissionProduct/GEF)

The GEF data has been saved as an Excel file to reduce the size and fit within GitHub's storage restrictions. Users who use the 46 group DPLS library structure can directly utilize this framework. GEF.py provides the user interface for the GEF data.

- Fission Product Estimation with Nagy Fits

(https://github.com/nickquartermont/NIF_ETA/tree/master/Models/FissionProduct/NagyFits)

The Nagy fit function requires input of the fissioning system or incident energy. Additional isotopes can be added directly to the Excel document containing the experimental data by following the same format. ETA_Nagy.py provides the user interface utilized to generate the fission products for ETA.

Bibliography

1. M. Chadwick and E. Al., “ENDF/B-VII.1 Nuclear Data for Science and Technology: Cross Sections, Covariances , Fission Product Yield,” *Nucl.Data Sheets*, vol. 112, no. 12, pp. 2887–2996, 2011.
2. Office of the Secretary of Defense, “Nuclear Posture Review,” 2018.
3. Department of Defense, “Summary of the 2018 National Defense Strategy of the United States of America.”
4. Joint Defense Science Board/Threat Reduction Advisory Committee Task Force, “The Nuclear Weapons Effects National Enterprise,” Office of the Under Secretary of Defense for Acquisition, Technology, and Logistics, Tech. Rep. June, 2010.
5. J. Bevins, “Targeted Modification of Neutron Energy Spectra for National Security Applications,” Ph.D. dissertation, University of California, Berkeley, 2017.
6. D. J. Trump, “State of the Union Address,” 2018.
7. Department of Defense, “Operation of the Defense Acquisition System (DOD Instruction 5000.02).”
8. Department of Defense, “DoD Nuclear Weapons Surety Program (DOD Directive 3150.02).”
9. J. C. Martz, “Without Testing: Stockpile Stewardship in the Second Nuclear Age,” Los Alamos National Lab.(LANL), Los Alamos, NM (United States), Tech. Rep., 2014.
10. Joint Defense Science Board Task Force, “Nuclear Weapon Effects Test, Evaluation, and Simulation,” Office of the Under Secretary of Defense for Acquisition, Technology, and Logistics, Tech. Rep. April, 2005.
11. *Nuclear Forensics: A Capability at Risk (Abbreviated Version)*. Washington, DC: The National Academies Press, 2010.
12. Joint Nuclear Forensics Working Group of the American Physical Society and the American Association for the Advancement of Science, “Nuclear Forensics: Role, State of the Art, and Program Needs.” Tech. Rep., 2013.
13. US National Security Council, “Review of the doe national security labs’ use of archival nuclear test data,” Committee on the Evaluation of Quantification of Margins and Uncertainties Methodology for Assessing and Certifying the Reliability of the Nuclear Stockpile, Letter Report, 2005.

14. V. Fedchenko, Ed., *The New Nuclear Forensics: Analysis of Nuclear Materials for Security Purposes*. Solna, Sweeden: Oxford University Press, 2015.
15. United Nations Scientific Committee on the Effects of Atomic Radiation, “Sources and Effects of Ionizing Radiation, vol. 1, Sources, 2000 Report to the General Assembly with Scientific Annexes, E.00.IX.3,” United Nations, New York, Tech. Rep., 2000.
16. C. J. Bridgman, *Introduction to the Physics of Nuclear Weapons Effects*. Fort Belvoir, VA: Defense Threat Reduction Agency, 2001.
17. Sandia National Laboratory, “Sun sets on Sandia Pulsed Reactor,” 2007.
18. United States Nuclear Regulatory Commission, “10 CFR Part 75: Safeguards on Nuclear Material,” 2018.
19. K. P. Carney, M. R. Finck, C. A. McGrath, L. R. Martin, and R. R. Lewis, “The Development of Radioactive Glass Surrogates for Fallout Debris,” *Journal of Radioanalytical and Nuclear Chemistry*, vol. 299, no. 1, pp. 363–372, 2014.
20. F. Dietrich and J. Escher, “Compound-nuclear Reaction Cross Sections via Surrogate Reactions,” *Nuclear Physics A*, vol. 787, no. 1, pp. 237 – 242, 2007, proceedings of the Ninth International Conference on Nucleus-Nucleus Collisions.
21. N. D. Scielzo *et al.*, “Statistical γ Rays in the Analysis of Surrogate Nuclear Reactions,” *Physical Review C - Nuclear Physics*, vol. 85, no. 5, 2012.
22. J. E. Escher, J. T. Burke, F. S. Dietrich, N. D. Scielzo, I. J. Thompson, and W. Younes, “Compound-nuclear reaction cross sections from surrogate measurements,” *Rev. Mod. Phys.*, vol. 84, pp. 353–397, Mar 2012.
23. N. Gharibyan, “Development af a fission-proxy method for the measurement of 14-MeV neutron fission yields at cams,” 10 2016.
24. N. Galy, N. Toulhoat, N. Moncoffre, Y. Pipon, N. Bérerd, M. R. Ammar, P. Simon, D. Deldicque, and P. Sainsot, “Ion Irradiation Used as Surrogate of Neutron Irradiation in Graphite: Consequences on ^{14}C and ^{36}Cl Behavior and Structural Evolution,” *Journal of Nuclear Materials*, vol. 502, pp. 20–29, 2018.
25. J. Bouchard and R. Heaphy, “QASPR Validation : Moving from Research Codes to Trusted Codes,” Sandia National Laboratories, Tech. Rep., 2007.
26. Y. Kasesaz and M. Karimi, “A Novel Design of Beam Shaping Assembly to use D-T Neutron Henerator for BNCT,” *Applied Radiation and Isotopes*, vol. 118, no. September, pp. 317–325, 2016.

27. I. M. Ardana and Y. Sardjono, "Optimization of a Neutron Beam Shaping Assembly Design for BNCT and Its Dosimetry Simulation Based on MCNPX," *Jurnal Teknologi Reaktor Nuklir Tri Dasa Mega*, vol. 19, no. 3, p. 121, 2017.
28. L. Zaidi, M. Belgaid, S. Taskaev, and R. Khelifi, "Beam Shaping Assembly Design of $^7\text{Li}(\text{p},\text{n})^7\text{Be}$ Neutron Source for Boron Neutron Capture Therapy of Deep-Seated Tumor," *Applied Radiation and Isotopes*, vol. 139, no. May, pp. 316–324, 2018.
29. J. E. Bevins, "Coeus V1.0," 2017. [Online]. Available: <https://github.com/SlaybaughLab/Coeus/releases>.
30. J. E. Bevins, S. Bogetic, L. A. Bernstein, R. Slaybaugh, and J. Vujic, "Meta-heuristic Optimization Method for Neutron Spectra Shaping," *Transactions of the American Nuclear Society*, vol. 118, pp. 455–458, 2018.
31. R. Stickney, Jason, "Pulse Height Spectra Analysis of a Neutron Energy Tuning Assembly," Ph.D. dissertation, Air Force Institute of Technology, 2018.
32. Department of Defense, "Nuclear Weapons Technology," in *Military Critical Technologies List*, 1998.
33. S. Glasstone and P. J. Dolan, *The Effects of Nuclear Weapons*, 3rd ed. Washington D.C.: United States Department Of Defense, 1977.
34. K. H. Schmidt, B. Jurado, C. Amouroux, and C. Schmitt, "General Description of Fission Observables: GEF Model Code," *Nuclear Data Sheets*, vol. 131, no. May, pp. 107–221, 2016.
35. S. Nagy, K. F. Flynn, J. E. Gindler, J. W. Meadows, and L. E. Glendenin, "Mass Distributions in Monoenergetic-Neutron-Induced Fission of U238," *Physical Review C*, vol. 17, no. 1, pp. 163–171, 1978.
36. L. Greenwood and C. Johnson, "Least-Squares Neutron Spectral Adjustment with STAYSL PNNL," *EPJ Web of Conferences*, vol. 106, p. 07001, 2016.
37. B. Rearden, M. Jessee, and Eds., *User Guide for the STAYSL PNNL Suite of Software Tools*, PNNL-22253, Pacific Northwest National Laboratory, Richland, WA, February 2013.
38. J. Turner, *Atoms, Radiation, and Radiation Protection*. Oak Ridge, TN: Wiley, 2008.
39. K. Krane, *Introductory Nuclear Physics*. New York: Jon Wiley & Sons, 1988.
40. H. Salmon, R. nal, B. Oruncak, U. Akcaalan, and H. A. Yalim, "(n,2n) and (n,3n) Neutron Induced Reaction Cross Sections above 8 MeV," *Acta Physica Polonica, A*, vol. 128, no. 2B, pp. B-231 – B-235, 2015.

41. A. Tonchev *et al.*, “Energy Evolution of the Fission-Product Yields from Neutron-Induced Fission of ^{235}U , ^{238}U , and ^{239}Pu : An Unexpected Observation,” in *The 6th International Conference on "Fission and Properties of Neutron-Rich Nuclei*, 2016.
42. J. Randrup and R. Vogt, “Nuclear Fission.” in *LLNL-BOOK-591732*. Lawrence Livermore National Laboratory, 2012.
43. K.-H. Schmidt and B. Jurado, “General Description of Fission Observables,” *JEFF Report 24*, 2014.
44. A. Nichols, D. Aldama, and M. Verpellis, “Handbook of Nuclear Data for Safeguards: Database Extensions,” International Atomic Energy Agency, Tech. Rep. August, 2008.
45. M. James, R. Mills, and D. Weaver, “A New Evaluation of Fission Product Yields and the Production of a New Library (UKFY2) of Independent and Cumulative Yields.” *Progress in Nuclear Energy*, vol. 26, no. 1, pp. 1 – 29, 1991.
46. E. Privas, G. Noguere, J. Tommasi, C. De Saint Jean, K.-H. Schmidt, and R. Mills, “Measurements of the Effective Cumulative Fission Yields of ^{143}Nd , ^{145}Nd , ^{146}Nd , ^{148}Nd and ^{150}Nd for ^{235}U in the PHENIX Fast Reactor,” *EPJ Nuclear Sciences & Technologies*, vol. 2, no. 32, pp. 1–16, 2016.
47. B. Singh, “Nuclear data sheets for $A = 89$,” *Nuclear Data Sheets*, vol. 114, no. 1, pp. 1 – 208, 2013.
48. D. A. Brown, E. A. Mccutchan, M. W. Herman, S. Hoblit, G. P. A. Nobre, and B. Pritychenko, “Uncertainty Quantification in the Nuclear Data Program,” *J. Phys. G: Nucl. Part. Phys.*, vol. 42, no. 034020, 2015.
49. F. Bostelmann and G. Strydom, “Nuclear Data Uncertainty and Sensitivity Analysis of the VHTRC Benchmark Using SCALE,” *Annals of Nuclear Energy*, vol. 110, pp. 317–329, 2017.
50. A. Knecht *et al.*, “Precision Measurement of the ^6He Half-Life and the Weak Axial Current in Nuclei,” *Phys. Rev. Lett.*, vol. 108, no. 122502, 2012.
51. R. Capote, K. Zolotarev, V. Pronyaev, and A. Trkov, “International Reactor Dosimetry and Fusion File IRDFF v.1.05,” *J. ASTM International*, vol. 9, no. 4, April 2012.
52. L. Greenwood, M. Kostal, S. Simakov, and A. Trkov, “Testing and Improving the International Reactor Dosimetry and Fusion File (IRDFF),” 2017.
53. K. I. Zolotarev and P. K. Zolotarev, “Evaluation of Some (n,n') , (n,γ) , (n,p) , $(n,2n)$ AND $(n,3n)$ Reaction Excitation Functions for Fission and Fusion Reactor

Dosimetry Applications," INDC International Nuclear Data Committee, Tech. Rep. INDC(NDS)-0657, 2013.

54. C. Diez, O. Cabellos, J. Martnez, and C. Ceresio, "Importance of nuclear data uncertainties in criticality calculations." *EPJ Web of Conferences*, vol. 27, p. 4, 2012.
55. D. Rochman, A. J. Koning, S. C. Van Der Marck, A. Hogenbirk, and C. M. Sciolla, "Nuclear data uncertainty propagation: Perturbation vs. Monte Carlo," *Annals of Nuclear Energy*, vol. 38, no. 5, pp. 942–952, 2011.
56. A. Aures, F. Bostelmann, M. Hursin, and O. Leray, "Benchmarking and Application of the State-of-the-art Uncertainty Analysis Methods XSUSA and SHARK-X," *Annals of Nuclear Energy*, vol. 101, pp. 262–269, 2017.
57. C. J. Díez, O. Buss, A. Hoefer, D. Porsch, and O. Cabellos, "Comparison of Nuclear Data Uncertainty Propagation Methodologies for PWR Burn-up Simulations," *Annals of Nuclear Energy*, vol. 77, pp. 101–114, 2015.
58. T. Zhu, A. Vasiliev, H. Ferroukhi, A. Pautz, and S. Tarantola, "NUSS-RF: Stochastic sampling-based tool for nuclear data sensitivity and uncertainty quantification," *Journal of Nuclear Science and Technology*, vol. 52, no. 7-8, pp. 1000–1007, 2015.
59. B. Rearden, M. Jessee, and Eds., *SCALE Code System*, ORNL/TM-2005/39 , Version 6.2.3, Oak Ridge National Laboratory, Oak Ridge Tennessee, March 2018, available from Radiation Safety Information Computational Center as CCC-834.
60. N. P. Luciano, "A High-Energy Neutron Flux Spectra Measurement Method for the Spallation Neutron Source," Master's thesis, University of Tennessee Knoxville, 2012.
61. E. E. Lewis and W. F. Millar Jr, *Computational Methods of Neutron Transport*. New York: John Wiley & Sons, 1984.
62. M. J. Wang, R. J. Sheu, J. J. Peir, and J. H. Liang, "Criticality Calculations of the HTR-10 Pebble-bed Reactor with SCALE6/CSAS6 and MCNP5," *Annals of Nuclear Energy*, vol. 64, pp. 1–7, 2014.
63. S. R. Johnson and K. T. Clarno, "Comparison of SCALE and MCNP Results for Computational Pebble Bed Benchmarks," *Trans. Am. Nucl. Soc.*, vol. 96, no. April, pp. 420–422, 2007.
64. Y. F. Chen, R. J. Sheu, S. H. Jiang, J. N. Wang, and U. T. Lin, "Surface Dose Rate Calculations of a Spent-Fuel Storage Cask by Using MAVRIC and Its Comparison with SAS4 and MCNP," *Nuclear Technology*, vol. 175, no. 1, pp. 343–350, 2011.

65. G. F. Knoll, *Radiation Detection and Measurement*, 4th Edition. Ann Arbor, MI: Wiley, 2010.
66. L. Kuijpers, R. Herzing, P. Cloth, D. Filges, and R. Hecker, “On the Determination of Fast Neutron Spectra with Activation Techniques; its Application in a Fusion Reactor Blanket Model,” *Nuclear Instruments and Methods*, vol. 144, no. 2, pp. 215–224, 1977.
67. E. Vagena, K. Theodorou, and S. Stoulos, “Thick-foils Activation Technique for Neutron Spectrum Unfolding with the MINUIT RoutineComparison with GEANT4 Simulations,” *Nuclear Instruments and Methods in Physics Research, Section A: Accelerators, Spectrometers, Detectors and Associated Equipment*, vol. 887, no. January, pp. 64–69, 2018.
68. M. Reginatto, “Overview of Spectral Unfolding Techniques and Uncertainty Estimation,” *Radiation Measurements*, vol. 45, no. 10, pp. 1323–1329, 2010.
69. F. G. Perey, *Least-Squares Dosimetry Unfolding: The Program STAY'SL (ORNL/TM-6062)*, Oak Ridge, Tennessee, 1977.
70. H. R. Vega Carrillo and M. P. I. De La Torre, “Catalogue to Select the Initial Guess Spectrum During Unfolding,” *Nuclear Instruments and Methods in Physics Research, Section A: Accelerators, Spectrometers, Detectors and Associated Equipment*, vol. 476, no. 1-2, pp. 270–272, 2002.
71. T. Goorley *et al.*, “Initial mcnp6 release overview,” *Nuclear Technology*, vol. 180, no. 3, pp. 298–315, 2012.
72. S. W. Mosher *et al.*, “ADVANTG: An Automated Variance Reduction Parameter Generator,” in *ORNL/TM-2013/416 Rev 1*, 2015.
73. O. Hurricane *et al.*, “Fuel gain exceeding unity in an inertially confined fusion implosion,” *Nature*, vol. 506, pp. 343–348, 01 2014.
74. C. B. Yeamans and B. E. Blue, “National Ignition Facility Neutron Sources,” Lawrance Livermore National Laboraotry, Tech. Rep., 2018.
75. K. C. Chen, H. Huang, and A. Nikroo, “Fabrication of Br-doped Glow Discharge Polymer (GDP) Capsules,” 2017.
76. H. Brysk, “Fusion Neutron Energies and Spectra,” *Plasma Physics*, vol. 15, no. 7, pp. 611–617, 1973.
77. B. Appelbe and J. Chittenden, “Relativistically Correct DD and DT Neutron Spectra,” *High Energy Density Physics*, vol. 11, no. 1, pp. 30–35, 2014.
78. X-5 Monte Carlo Team, “MCNP - A General Monte Carlo N-Particle Transport Code, Version 5,” *LA-UR-03-1987*, 2008.

79. E. I. Moses *et al.*, “Overview: Development of the National Ignition Facility and the Transition to a User Facility for the Ignition Campaign and High Energy Density Scientific Research,” *Fusion Science and Technology*, vol. 69, no. 1, pp. 1–24, 2016.
80. D. Campolina and J. Frybort, “Uncertainty Propagation for Lwr Burnup Benchmark Using Sampling Based Code Scale/Sampler,” *Acta Polytechnica CTU Proceedings*, vol. 14, p. 8, 2018.
81. D. Rochman, A. Vasiliev, H. Ferroukhi, T. Zhu, S. C. Van Der Marck, and A. J. Koning, “Nuclear Data Uncertainty for Criticality-Safety: Monte Carlo vs. Linear Perturbation,” *Annals of Nuclear Energy*, vol. 92, pp. 150–160, 2016.
82. M. Griseri, L. Fiorito, A. Stankovskiy, and G. Van den Eynde, “Nuclear Data Uncertainty Propagation on a Sodium Fast Reactor,” *Nuclear Engineering and Design*, vol. 324, no. February, pp. 122–130, 2017.
83. W. Wieselquist, T. Zhu, A. Vasiliev, and H. Ferroukhi, “PSI Methodologies for Nuclear Data Uncertainty Propagation with CASMO-5M and MCNPX: Results for OECD/NEA UAM Benchmark Phase I,” *Science and Technology of Nuclear Installations*, vol. 2013, 2013.
84. T. Zhu, A. Vasiliev, H. Ferroukhi, and A. Pautz, “NUSS: A Tool for Propagating Multigroup Nuclear Data Covariances in Pointwise ACE-formatted Nuclear Data Using Stochastic Sampling Method,” *Annals of Nuclear Energy*, vol. 75, pp. 713–722, 2015.
85. M. L. Williams *et al.*, “A Statistical Sampling Method for Uncertainty Analysis with SCALE and XSUSA,” *Nuclear Technology*, vol. 183, no. 3, pp. 515–526, 2013.
86. G. Zerovnik, R. Capote, and A. Trkov, “On Random Sampling of Correlated Resonance Parameters with Large Uncertainties,” *Nuclear Instruments and Methods in Physics Research, Section A: Accelerators, Spectrometers, Detectors and Associated Equipment*, vol. 723, pp. 89–98, 2013.
87. K. Schmidt *et al.*, “General Description of Observables in Low-energy Fission : GEF Model Code,” 2015.
88. L. Glendenin, J. Gindler, D. Henderson, and J. W. Meadows, “Mass Distributions for Monoenergetic-Neutron-Induced Fission of ^{235}U ,” *Physical Review C*, vol. 24, no. 6, pp. 2600–2605, 1981.
89. G. P. Ford and R. B. Leachman, “Fission Mass Yield Dependence on Angular Momentum,” *Physical Review*, vol. 137, no. 4 B, 1965.

90. M. E. Gooden *et al.*, “Energy Dependence of Fission Product Yields from ^{235}U , ^{238}U and ^{239}Pu for Incident Neutron Energies Between 0.5 and 14.8 MeV,” *Nuclear Data Sheets*, vol. 131, pp. 319–356, 2016.
91. M. E. Gooden, “Energy Dependence of Fission Product Yields from ^{235}U , ^{238}U , and ^{239}Pu for Incident Neutron Energies Between 0.5 and 14.8 MeV,” Ph.D. dissertation, North Caroline State University, 2014.
92. D. R. Nethaway and G. Barton, “A Compilation of Fission Product Yields in use at the Lawrence Livermore Labratory,” Tech. Rep., 1973.
93. C. Chapman, T and G. A. Anzelon, “Fission Product Yields from 6-9 MeV Neutron Induced Fission of U-235 and U-238,” *Physical Review C*, vol. 17, no. 3, pp. 1089–1097, 1978.
94. T. R. England and B. F. Rider, “Evaluation and Compliation of Fission Product Yields,” *La-Ur-94-3106*, pp. 1–173, 1994.
95. J. G. Cunningham, J. A. B. Goodall, and H. H. Harris, “Absolute Yields in the Fission of ^{235}U By Mono-Energetic Neutrons of Energy 130-1700 keV,” *J. Inorg. Nucl. Chem.*, vol. 36, no. 7, pp. 1453–1457, 1974.
96. J. R. Taylor, *An Introduction to Error Analysis: The Study of Uncertainties in Physical Measurements*, 2nd ed. South Orange, NJ: University Science Books, 1997.
97. H. G. Norment, “DELFIC: Department of Defense Fallout Prediction System.” in *Fundamentals, vol. I. Atmospheric Science Associates*. Bedford MA: ADA 088 367, 1979.

REPORT DOCUMENTATION PAGE

*Form Approved
OMB No. 0704-0188*

The public reporting burden for this collection of information is estimated to average 1 hour per response, including the time for reviewing instructions, searching existing data sources, gathering and maintaining the data needed, and completing and reviewing the collection of information. Send comments regarding this burden estimate or any other aspect of this collection of information, including suggestions for reducing this burden to Department of Defense, Washington Headquarters Services, Directorate for Information Operations and Reports (0704-0188), 1215 Jefferson Davis Highway, Suite 1204, Arlington, VA 22202-4302. Respondents should be aware that notwithstanding any other provision of law, no person shall be subject to any penalty for failing to comply with a collection of information if it does not display a currently valid OMB control number. PLEASE DO NOT RETURN YOUR FORM TO THE ABOVE ADDRESS.

1. REPORT DATE (DD-MM-YYYY)	2. REPORT TYPE		3. DATES COVERED (From — To)		
19-15-2011	Master's Thesis		Jan 2010 — Aug 2011		
4. TITLE AND SUBTITLE			5a. CONTRACT NUMBER 5b. GRANT NUMBER 5c. PROGRAM ELEMENT NUMBER		
Effect of Storm Enhanced Densities on Geo-Location Accuracy Over CONUS					
6. AUTHOR(S)			5d. PROJECT NUMBER 5e. TASK NUMBER 5f. WORK UNIT NUMBER		
Capt Lindon H. Steadman					
7. PERFORMING ORGANIZATION NAME(S) AND ADDRESS(ES)				8. PERFORMING ORGANIZATION REPORT NUMBER	
Air Force Institute of Technology Graduate School of Engineering and Management (AFIT/EN) 2950 Hobson Way WPAFB OH 45433-7765				AFIT/GAP/ENP/11-S01	
9. SPONSORING / MONITORING AGENCY NAME(S) AND ADDRESS(ES)				10. SPONSOR/MONITOR'S ACRONYM(S)	
Air Force Weather Agency 101 Nelson Drive Offutt AFB, NE 68113 DSN 271-0690, COMM 402-294-0690 Email: 2syosdor@offutt.af.mil				AFWA	
				11. SPONSOR/MONITOR'S REPORT NUMBER(S)	
12. DISTRIBUTION / AVAILABILITY STATEMENT					
APPROVED FOR PUBLIC RELEASE; DISTRIBUTION UNLIMITED.					
13. SUPPLEMENTARY NOTES					
14. ABSTRACT					
Storm enhanced densities (SEDs) are ionospheric plasma enhancements that disrupt radio communications in the near-Earth space environment, degrading the Global Positioning System (GPS) and other high-frequency systems. Accurate GPS/total electron content (TEC) correction maps produced by ionosphere models can mitigate degradations from SEDs. An artificial SED was created and ingested via slant TEC measurements into the Global Assimilation of Ionospheric Measurements Gauss-Markov Kalman Filter Model to determine how many ground GPS receivers are needed to produce reliable GPS/TEC correction maps over the continental United States during geomagnetic storming. It was found that 110 well-positioned GPS receivers produced the best overall TEC accuracy, although significantly improved accuracy was still achieved if 40 or more receivers were used. It was determined that receiver positioning had a greater impact on TEC accuracy than the number of receivers. Additionally, it was found that TEC accuracy for the SED region increased at the expense of TEC accuracy everywhere else on the map.					
15. SUBJECT TERMS					
Ionosphere, Ionosphere Forecast Model, Global Assimilation of Ionospheric Measurements Gauss-Markov Kalman Filter Model, Space Weather					
16. SECURITY CLASSIFICATION OF:			17. LIMITATION OF ABSTRACT	18. NUMBER OF PAGES	19a. NAME OF RESPONSIBLE PERSON Lt Col Ariel O. Acebal, AFIT/ENP
a. REPORT	b. ABSTRACT	c. THIS PAGE	U	110	19b. TELEPHONE NUMBER (include area code) (937) 255-3636, x4518; ariel.acebal@afit.edu

0.149
0.0193
0.783
0.0485
0.000324

0.126
0.0131
0.823
0.0380
0.0000723
19 EN 4 L 36 A7 24